AIAA JOURNAL
Vol. 48, No. 4, April 2010

Application of Inlet Injection to a Three-Dimensional Scramjet at Mach 8

James C. Turner* and Michael K. Smart†
University of Queensland, Brisbane, Queensland 4072, Australia

DOI: 10.2514/1.J050052

An investigation of inlet injection in a scramjet having a three-dimensional inlet and an elliptical combustion was undertaken. Experiments were conducted using a test flow simulating a Mach 8.1 flight condition with an altitude of 32 km. The objective was to determine the feasibility of reducing the combustion-chamber length by injection of hydrogen fuel in the inlet. The study involved a self-starting three-dimensional inlet with an overall geometric contraction ratio of 5.80, of which 2.08 was internal. The fuel was injected through multiple portholes in the forward portion of the inlet to allow significant mixing upstream of the combustion chamber. The divergent elliptical combustion chamber had a length sized for fuel ignition and combustion only and used a fluid-dynamic ignition scheme requiring no physical obstructions to the flowpath. Results indicated that inlet injection produced robust combustion at good combustion efficiency over a large fueling range up to an equivalence ratio of 0.92. A further key result was that no evidence of combustion was observed in the inlet. These experiments suggest that fuel injection in the inlet is a promising concept for higher-speed scramjet applications.

Nomenclature

A	=	area, m^2
C_{Di}	=	inlet drag coefficient
C_f	=	skin-friction coefficient
C_h	=	heat transfer coefficient
h	=	combustion-chamber entrance height, mm
l_c	=	combustion-chamber length, m
M	=	Mach number
m_c	=	mass capture ratio
p	=	pressure, kPa
$T_{\text{potential}}$	=	thrust potential, N
x	=	axial distance, m
ΔD	=	inlet drag increase due to inlet injection, N
φ	=	fuel equivalence ratio

Subscripts

i	=	inlet
max	=	maximum
s	=	nozzle stagnation condition
t	=	pitot
1	=	inlet entrance
4	=	combustion-chamber exit
0	=	flight condition

I. Introduction

HIGH-SPEED flight within the atmosphere has applicability to transport, defense, and space access [1,2]. To date, the two most successful propulsion systems are the rocket and the conventional ramjet. Rockets are particularly useful for space access, as they do not rely on atmospheric oxygen for combustion. However, for operation wholly within the atmosphere, the need to carry oxidizer leads to a severe tradeoff between range and payload mass. For this reason, airbreathing propulsion is attractive for atmospheric flight. The conventional ramjet, which relies on a subsonic combustion process, reaches the limit of its operational envelope at a Mach number of about 6. This is due mainly to effects associated with the high gas temperatures attained in slowing the freestream to subsonic speeds for combustion. For higher Mach number flight, the supersonic combustion ramjet or scramjet has shown considerable promise [2]. In a scramjet, the problems that plague the conventional ramjet at higher Mach numbers are avoided by maintaining a supersonic flow throughout the engine. However, the high velocities in the scramjet combustion chamber pose great challenges for mixing and combustion of fuel within desirable length scales.

A scramjet consists of three main components: 1) the inlet, which captures the air and facilitates compression, 2) the combustion chamber, which contains the heat addition from combustion of fuel, and 3) the nozzle, which expands the processed air for thrust production. Furthermore, in an airframe-integrated scramjet such as shown in Fig. 1, both the vehicle forebody and its aft surfaces perform part of the compression and expansion, respectively. In these engines, the length of the inlet and nozzle are dictated by aerodynamic considerations (which depend largely on flight Mach number) and the required contraction ratio of the engine. In some instances, the inlet can be up to half the flowpath length. The combustion-chamber length is set by the length needed to mix fuel and air, plus the time needed to ignite and complete the combustion reaction. As heating rates and drag per unit surface area are greatest in the combustion chamber, its length must be kept to a minimum. Figure 1 also shows the scramjet station notation used in this paper.

Many different strategies have been developed to facilitate fuel/air mixing and combustion heat release for scramjet applications [3]. These have involved fuel injection through flush wall holes [4–8] or, alternatively, fuel injection in combination with physical obstructions to the flow such as cavities [9,10], struts [11], or ramps [12,13]. An alternative methodology that has attracted recent attention is the possibility of moving fuel injection to the inlet [14–17]. This concept has the important advantage of significantly increasing the mixing length for fuel and air, without increasing the overall length of the engine (as the inlet is already required for compression). In such a configuration, the fuel can be significantly mixed before it reaches the combustion chamber, and combustion-chamber length can then be determined simply by the time needed to ignite and complete the combustion reaction. Possible disadvantages of this idea are 1) disruption or changes to the operation of the inlet and 2) preignition of fuel on the forward-facing inlet surfaces and consequent drag generation. While these phenomena may limit the general applicability of this concept, the potential benefits of inlet

Received 8 July 2009; revision received 26 October 2009; accepted for publication 5 November 2009.

*Ph.D. Candidate, Centre for Hypersonics, Division of Mechanical Engineering.

†Professor, Centre for Hypersonics, Division of Mechanical Engineering. Senior Member AIAA.

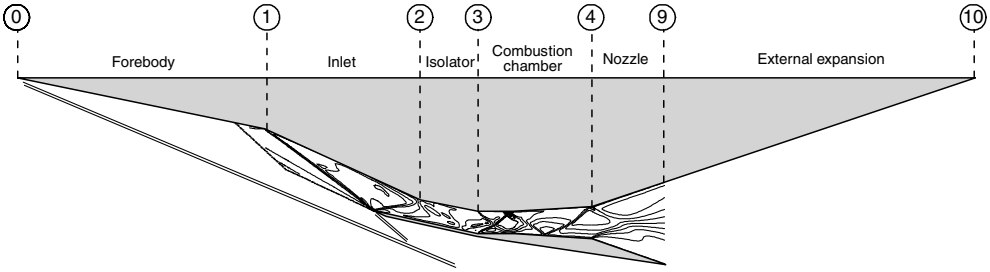

Fig. 1 Schematic of an airframe-integrated scramjet.

injection (particularly at high hypersonic speeds, at which mixing-length requirements dominate combustion-chamber length) warrant its investigation.

Previous studies of inlet injection have been concentrated at Mach 8 and above and have involved flush wall injection in the inlet and the use of a fluid-dynamic ignition scheme known as radical farming. This ignition methodology does not require physical obstructions in the combustion chamber, but relies on the structure of oblique shocks and expansions in the flow to generate local high-temperature regions. An early investigation of radical farming by Gardner et al. [15], using the concept shown in Fig. 2, demonstrated the ability to inject gaseous hydrogen fuel in the inlet and achieve ignition and combustion in the combustion chamber without ignition in the inlet. The experiments were conducted in a shock tunnel at a total enthalpy equivalent to flight at Mach 8 (3 MJ/kg), with the model wall temperature remaining close to 300 K throughout the test time.

The radical-farming concept was examined further by Odam [16] and Odam and Paull [16,18], who used an adjustable 2-D scramjet to determine the minimum contraction ratio that would support combustion of gaseous hydrogen at similar total enthalpy to that of Gardner et al. [15]. This experimental study indicated that the combination of inlet injection and radical farming enabled robust combustion at relatively low inlet contraction ratio without the use of physical flame holders. A recent numerical study of a 2-D radical-farming scramjet by McGuire [17] showed that the likely ignition mechanism in these engines is the transit of premixed fuel through small separations caused by shock/boundary-layer interactions. By tracing a streamline though such a region it was shown that the residence time in the high-temperature separation was sufficient to promote ignition. This study suggested ignition can be achieved in hot regions near walls and that ignition is significantly enhanced by the presence of small separated regions.

The research described in the current paper involved shock-tunnel experiments of inlet injection in a 3-D scramjet. The inlet geometry used for the study was based on the rectangular-to-elliptical shape transition (REST) configuration of Smart [19]. This fixed-geometry mixed-compression configuration transitions smoothly from a quasi-rectangular capture shape to an elliptical throat. In combination with a divergent elliptical combustion chamber, REST inlets have been shown to produce a useful flowpath for hypersonic applications [20]. The current configuration is an exploratory Mach 8.1 design-point flowpath which has been explicitly adapted to be used in conjunction with inlet injection and radical farming. The fuel of choice was gaseous hydrogen.

The paper first describes the design methodology used for the inlet, combustion chamber, and nozzle that make up the engine, followed by a description of the experimental model and the T4 shock tunnel. Initial experimental results for the unfueled flowpath are presented next, with comparisons to numerical simulations. The fueled results are then presented along with some corresponding cycle analysis. The paper closes with some conclusions about the experimental results and the applicability of inlet injection to 3-D scramjets.

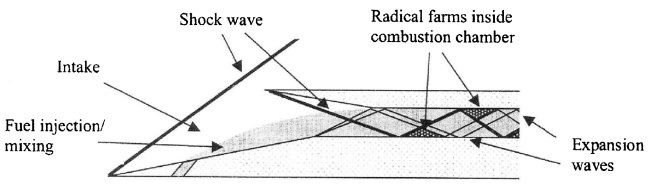

Fig. 2 Radical farming scramjet (source: Gardner et al. [15]).

II. Flowpath Design

The simulated flight condition chosen for the current study was Mach 8.1 at an altitude of 32 km. This is a typical test point that has been generated in flight tests undertaken by the University of Queensland's HyShot program [21] and was chosen with this in mind. The contraction ratio of the engine was determined by assuming the presence of a 6° forebody wedge in front of the inlet and the requirement that the flow entering the combustion chamber be at approximately 50 kPa. Assuming that air behaves as a calorically perfect gas with a ratio of specific heats of 1.4, flow processed by the forebody shock will enter the inlet module at Mach 6.71 in this instance. If an efficient inlet geometry is used, this will result in a mean flow static temperature well below the self-ignition temperature of hydrogen, so radical farming or some other methodology is needed to establish robust combustion. An aspect ratio of 1.80 was chosen for the elliptical combustion chamber, and an engine capture width of 120 mm (based on the expected core flow of the shock tunnel) set the scale of the experiments.

A. REST Inlet with Inlet Injection

The design methodology used for REST inlets [18] makes use of streamline-tracing techniques. A capture shape is first established, as is an axisymmetric compression flowfield that has the same compression ratio as is required for the inlet. Streamlines passing through the edges of the capture shape and the elliptical throat are then traced through the flowfield, and these sets of streamlines are lofted together to provide a smooth transition between the capture shape and the elliptical throat. Finally, a viscous correction is added to the internal shape and checks are made to confirm that there are no regions where shock-induced boundary-layer separations can occur. The resulting inlets have highly swept leading edges and a notched cowl, leading to moderate internal contraction ratio. This enables the inlets to be self-starting without the need for variable geometry.

The usual design process for a REST inlet is motivated by the desire to reduce losses in the inlet due to both viscous effects and shock waves and to minimize flow nonuniformities at the inlet exit plane through shock cancellation. However, for an engine with inlet injection and radical farming, this process had to be adapted to produce a distinctly nonuniform flow entering the combustion chamber. This was achieved by designing the inlet for an inflow Mach number lower than that of the desired operating condition. Figure 3 shows a schematic of a REST inlet with flow at its design Mach number (shock cancellation at the throat) and with flow faster than its design Mach number, or oversped. In the oversped condition, the cowl shock that reflects back toward the body side of the inlet impinges downstream of the throat and is not canceled. This generates shocks and expansions that propagate past the inlet exit and into the combustion chamber.

The presence of interactions RC1 and RB2, although beneficial for the ignition process, can potentially lead to excessive wall heating due to shock focusing. In the case of RB2, the heat transfer to the walls is not significantly greater than other interactions in the engine.

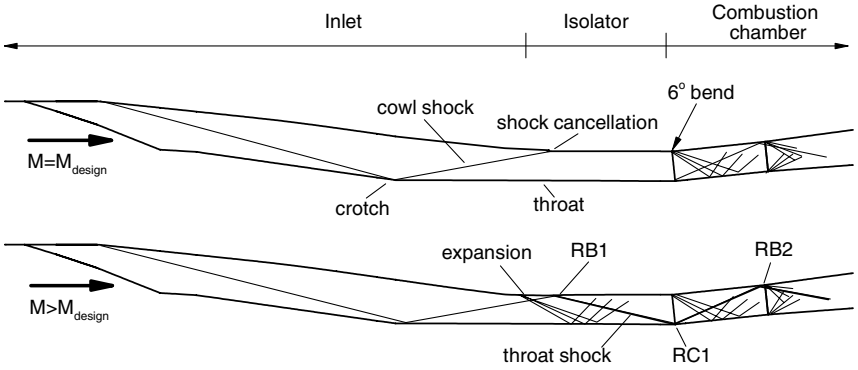

Fig. 3 Schematic of the main shock structure in the inlet and combustion chamber for on-design inlet (top) and oversped inlet (bottom).

This is largely due to the fact that the shocks are nonplanar and the focusing is only evident around the centerline of the scramjet. This coincides with the thick body-side boundary layer, which tends to reduce the heat transfer. The RC1 interaction is more problematic: the flow at this location has a higher density and a thinner boundary layer, resulting in an elevated heat transfer. Fortuitously, this interaction is on the cowl side of the scramjet, where a high-temperature wall can potentially radiate heat from the exterior of the vehicle. This is an active area of research and requires the use of ultra-high-temperature materials in the structure.

For the current flowpath, a design point of Mach 6.0 was chosen for the Mach 6.71 test condition. This condition would cause the initial shock in the inlet to impinge on the wall downstream of the cowl. Such a shock interaction has the potential to reduce the inlet efficiency and cause excessive heating, particularly at the crotch. In order to avoid this, the cowl leading edges were cut back to reside behind the inlet shock. This allowed the inlet to operate at Mach 6.71, with a small amount of spillage to avoid swallowing the initial shock. The final REST inlet geometry created for the current study had an overall geometric contraction ratio of 5.80 and an internal contraction ratio of 2.08. Experimental testing of a previous REST inlet with an internal contraction ratio of 2.15 at Mach 6.12 [22] showed that it was self-starting. Based on this information, the current REST inlet was also expected to be self-starting.

B. Elliptical Combustion Chamber

The radical-farming concept was employed as the ignition methodology for the flowpath. This required generation of shocks and expansions in the inlet that were then manipulated in the combustion chamber to create high-temperature ignition zones as close as possible to the entrance of the combustion chamber while avoiding large-scale boundary-layer separation and flowpath blockage. The main considerations for the design of the combustion chamber were as follows:

1) Manipulate the shocks and expansion waves to create local fluid-dynamic ignition zones.

2) Determine the length required for ignition and combustion, assuming the fuel and air entering the combustion chamber are premixed.

3) Choose an axial area distribution to enable combustion at equivalence ratios close to 1.0.

As is typical of many scramjet designs, the combustion chamber in the current flowpath was required to be parallel with the nominal flight velocity. A 6° bend was therefore placed at the start of the combustion chamber to accomplish this, as shown in the schematic of Fig. 3. The isolator length between the inlet throat and the bend was chosen to reinforce the strength of the reflected throat shock. This positioning created two shock-interaction zones that may be favorable to ignition, labeled RC1 (*first* shock *reflection* on the *cowl side* of the engine) and RB2 (*second* shock *reflection* on the *body side* of the engine) in Fig. 3. Inlet injection in these experiments was on the body side; hence, interaction RC1 on the cowl side of the flowpath was expected to have very low fuel concentration. Interaction RB2 on the body side of the combustion chamber slightly downstream of the bend was considered the most promising site for ignition.

Given the assumption that fuel entering the combustion chamber is essentially premixed, combustion-chamber length requirements were governed by the ignition and reaction times for the combustion process, rather than fuel/air mixing lengths. Ignition and reaction times were estimated here using correlations of Pergament [23] for reaction of hydrogen in air. Given the assumption of supersonic flow through the combustion chamber (in this case, a velocity of 2400 m/s was used), the length required for the ignition and reaction phases was calculated for a range of static temperatures and pressures. Curves of ignition and reaction length for representative pressures of 50 and 100 kPa are shown in Fig. 4. As can be seen, ignition length depends mainly on temperature, whereas reaction length depends strongly on both temperature and pressure. With the assumption that the engine will generate hot regions in the

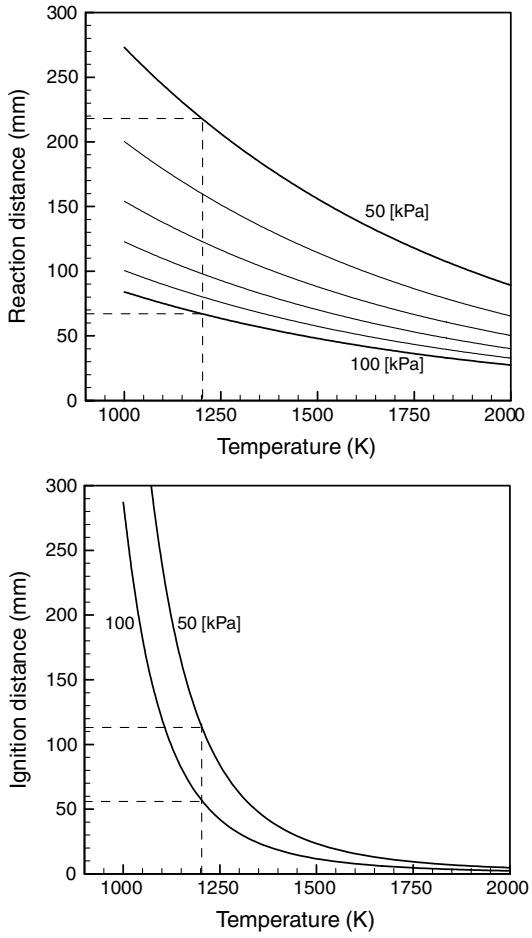

Fig. 4 Ignition and reaction lengths of hydrogen assuming a combustion-chamber velocity of 2400 m/s.

combustion chamber with temperatures in the vicinity of 1200 K, hydrogen ignition length decreases from 112 to 56 mm as the pressure increases from 50 to 100 kPa, while reaction length decreases from 218 to 66 mm for the same pressure range. In the absence of any further knowledge of how the combustion will occur, a mean combined ignition and reaction length of 226 mm was used to set the combustion-chamber length. Assuming ignition occurs at RB2 (Fig. 3), this resulted in an overall combustion-chamber length of $l_c = 305$ mm. For reference, the height of the ellipse at the start of the combustion chamber was $h = 30.1$ mm, which results in an l_c/h for the combustion chamber of 10.13.

The cross-sectional area distribution along the axis of the combustion chamber strongly influences its pressure distribution. Ideally, the area distribution would be matched to the axial heat-release profile of the combustion process to prevent an excessive pressure rise and boundary-layer separation, while maintaining high enough pressure for short combustion ignition/reaction length. Without prior knowledge of the rate of heat release through the combustion chamber, specifying an area distribution is not straightforward. Given the exploratory nature of this study, a combustion-chamber area ratio of 2.0 was chosen, with an initial constant-area section of length $1.0h$, followed by a linear increase of the ellipse axes that maintained the aspect ratio throughout.

C. Generic Nozzle

A simple elliptical thrust nozzle was included in the flowpath to provide a means of determining the relative thrust of different fuel-injection schemes and fuel equivalence ratios. It was a simple ruled surface with an area ratio of 5.0 and an expansion half-angle of 10°. As such, the internal thrust calculated in these experiments is indicative of performance only and can be viewed as a thrust potential rather than the actual thrust generated by an engine integrated into a flight vehicle with optimized expansion.

III. Experimental Model

A. Flowpath

Three views of the experimental model are shown in Fig. 5, with key dimensions indicated. The REST inlet was machined from a polymer material NECURON® 651.[‡] Although the maximum working temperature of this material is only 70°C, testing showed that during the very brief test time, the model did not heat up sufficiently to cause melting. The leading edges of the inlet are blunted with a radius of 0.7 mm. The width of the inlet was 120 mm and the capture area was 7385 mm^2. A total of 11 static-pressure taps were placed along the centerline of the inlet on the body side only. A rectangular hole was machined into the external compression surface to allow for the inlet injector plenum to be installed flush. Note that a short forebody with 77 mm length and 0.7 mm leading-edge radius was installed ahead of the inlet to generate an incoming boundary layer.

The combustion chamber was also machined from NECURON® 651. A total of 20 static-pressure taps were machined along the combustion-chamber centerline: 10 on the body-side wall and 10 on the cowl side. The elliptical nozzle was manufactured using the selective-laser-sintering process from the nylon–glass material CapForm™. The internal surface was finished using a cyanoacrylate coating to provide a smooth internal surface. A total of 16 static-pressure taps were placed in the nozzle: eight on the body-side wall and eight on the cowl side.

B. Fuel System

Fuel injection into the inlet was at a location 275 mm from the leading edge of the forebody, as shown in Fig. 5. Injection was by means of three 2.2-mm-diam portholes placed at 25 mm lateral spacing and directed 45° to the local flow in the downstream direction. To determine the mass flow rate, the fuel flow was stagnated just before injection. In this way, the mass flow rate through

[‡]Data available online from http://www.necumer.de [retrieved 12 Dec. 2007].

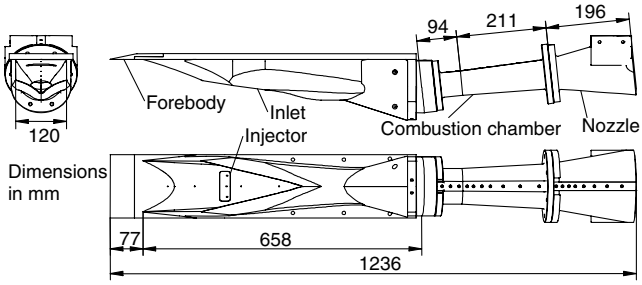

Fig. 5 Schematic diagram of REST scramjet model.

the sonic injectors was determined by calculating a loss coefficient for the injector holes. Stagnation pressures for injection were approximately 3 MPa for high equivalence ratios. To contain these pressures, an aluminum manifold was used for a plenum chamber.

The fuel reservoir used in the experiments consisted of a 12.2-mm-diam Ludwieg tube initially filled to a pressure slightly higher than that required in the fuel plenum chamber. Several milliseconds before the onset of the test flow, a fast-acting valve that separated the plenum chamber from the Ludwieg tube was opened. The fuel then filled the plenum chamber and flowed from the injectors. The fast-acting valve was a 1/2 in. Joucomatic™ ASCO solenoid valve model SC B223A103 and it was typically kept open for 30 ms, spanning the duration of the test run. The length of the Ludwieg tube was 1419 mm, sufficiently long for the reflected expansion wave from the closed end to not propagate into the plenum chamber during the test time. This allowed for a pressure plateau in the plenum chamber and, consequently, a constant mass flow rate from the injectors during the test time.

C. Instrumentation

Pressure transducers were mounted behind the static-pressure taps along the model walls. The taps were 2-mm-deep holes to ensure a fast response to the rapidly changing pressures during the test. The pressure transducers used in this application were the Kulite™ XTEL-190M series with ranges of 10, 25, or 100 psi. These transducers measure absolute pressure and had a calibration error of $\pm 1\%$ of full scale, with natural frequencies of 175, 240, and 380 kHz, respectively. In addition, a single pitot probe was mounted above the forebody to monitor the test flow condition. This probe used a PCB™ model 111A26 piezoelectric pressure transducer with calibration error of $\pm 2\%$ of full scale and a natural frequency of greater than 400 kHz. A 12-bit transient digital data acquisition and storage unit with a sampling time of 1 μs was used to record the data sets.

IV. Facility and Test Conditions

The T4 free-piston shock-tunnel facility [24] was used for the experimental investigation. It consists of four main sections: high-pressure reservoir, compression tube, shock tube, and test section, as shown in Fig. 6. A shock wave generated in the test gas contained in the shock tube increases its pressure and temperature. Reflection of the shock wave from the end of the shock tube stagnates the test gas, which subsequently expands through the nozzle producing a high-speed test flow of several milliseconds' duration. This process allows the high stagnation enthalpies that are characteristic of hypersonic flight to be reproduced, which is of primary importance in combustion experiments.

For the current experiments, the tunnel was configured as a semi-free-jet facility, in which the flow exiting the nominal Mach 6 nozzle was intended to replicate the Mach number, static pressure, and temperature on the 6° forebody of a flight vehicle. Table 1 lists the properties for the target and simulated conditions. The target flight condition (column 1) was calculated for an altitude of 30 km and is shown along with corresponding properties on a 2-D 6° wedge forebody (column 2). Column 3 of Table 1 lists the typical properties generated by the T4 facility at the nozzle exit for the current experiments. Mach number and static temperature closely simulate

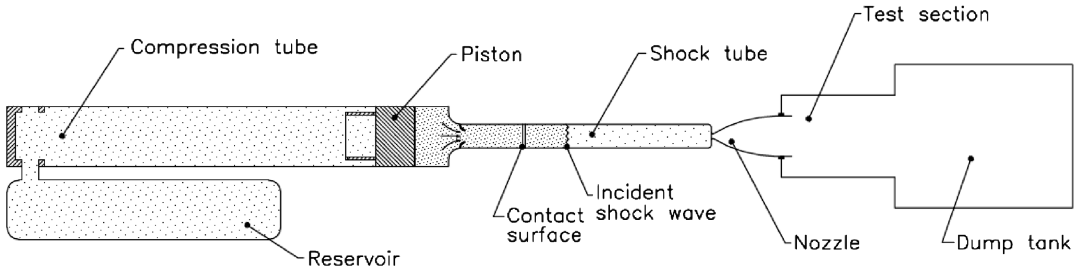

Fig. 6 Components of the T4 reflected shock tunnel [25].

vehicle forebody conditions, and static pressure is approximately 75% of the target. This corresponds to a simulated altitude of 32 km, slightly higher than the target but still well within the flight-test envelope. These nominal facility test properties were calculated using the quasi-1-D nonequilibrium nozzle code NENZF [26], which was run to match the measured ratio of pitot-to-supply pressure (p_t/p_s) for the nozzle. These properties were determined by averaging over a set of test runs.

Figure 7 shows pitot- and static-pressure time histories for a typical experiment during the test program. The onset of flow in the test section is indicated by the sharp rise in pressure at 1 ms. This was followed by a period of unsteady flow establishment in the divergent section of the facility nozzle. At the end of the flow-establishment time, the steady test time began. The end of the test time was the end of the steady period of test flow, as this lead to a reduction in the mass flow rate of air through the model. At this condition, this occurs before significant contamination of the test gas by the argon driver gas [27,28], giving approximately 2 ms of usable test time.

V. Numerical Simulation and Cycle Analysis

Numerical simulations of the unfueled flowpath were conducted with the NASA Langley Research Center's hypersonic code VULCAN [29]. This code uses an upwind, cell-centered, numerical scheme to solve the compressible Navier–Stokes equations over a computational domain that included the internal flowpath of the scramjet in addition to that of the experimental forebody and external flow around the cowl leading edges. The computational domain consisted of a structured grid with a total of 40 blocks: 20 for the inlet and associated inflow, and 16 for the external flow region. Of the remaining four blocks, three where used for the combustion chamber and one was used for the nozzle. Grid clustering was used at wall boundaries; however, wall functions were also applied [29]. This allowed the boundary layer to be resolved for wall cells with a y^+ of 6 or greater. The y^+ of the inlet grid wall cells was typically less than 25 and of the thrust nozzle was less than 60. Despite this, the overall size of the grid was just over 5.6 million cells, which placed significant demands on the computational resources available.

The numerical scheme implemented was based on the REST inlet study of Smart and White [30]. Convection terms were treated using the low-dissipation Edwards flux-splitting scheme with a van Leer limiter. Wilcox's modified k-ω turbulence model was used with Reynolds stresses calculated using Boussinesq model terms. In all simulations, the flow was assumed to be turbulent throughout the computational domain. The scramjet surfaces were modeled with isothermal wall boundary conditions having a temperature of 300 K. This is representative of the physical situation during a short-duration test, in which the model walls have insufficient time to rise above ambient temperature. The inflow conditions for the computational domain were assumed to be uniform and were identical to the experimental test flow condition listed in Table 1.

Analysis of combustion in the experimental model involved quasi-one-dimensional cycle methods. Although the real combusting flow was far from uniform at any cross section, when used correctly, these techniques provided an efficient means of determining the performance of an engine. To this end, extraction of the 3-D numerical simulation data used for inflow conditions was based on stream-thrust averaging across the inlet throat cross section, where flow distortion was minimal [31]. The cycle-analysis code [32] used enabled prediction of the pressure distribution in the regions of the engine affected by combustion, therefore enabling comparison with experimental data. It was based on the classical gasdynamic methods presented by Shapiro [33], but with the flow modeled as a mixture of thermally perfect gases that are in thermal equilibrium. Both skin-friction drag and heat transfer to the wall were estimated with uniform skin-friction and heat transfer coefficients. The area distribution of the combustion chamber was known a priori, and the amount of fuel allowed to react with the air at a particular station was dictated by a user-defined combustion-efficiency curve. This combustion-efficiency-curve models both the mixing and kinetic aspects of the engine and was adjusted to match the measured pressure distributions. Accurate knowledge of the mass flow rate, momentum flux, and specific total enthalpy of both the incoming air and fuel are needed for meaningful results to be obtained. The key limitation of the code for scramjet applications was the assumption of quasi-one-dimensional flow.

Table 1 Simulated flight and experimental conditions

		Flight		
Parameter	Units	Freestream	Forebody	Experiment
Mach no.	——	8.1	6.71	6.6
Static temperature	K	227	320	340
Static pressure	kPa	1.2	3.6	2.63
Static density	$\mathrm{kg\,m^{-3}}$	0.018	0.040	0.027
Velocity	$\mathrm{m\,s^{-1}}$	2439	2400	2448
Stagnation enthalpy	$\mathrm{MJ\,kg^{-1}}$	3.2	3.2	3.34
Stagnation pressure	MPa	19.9	18.0	12.6
Unit Reynolds no.	$\mathrm{m^{-1}}$	3.0×10^6	5.0×10^6	4.5×10^6

VI. Results and Discussion

Tests were conducted to ascertain the performance of the flowpath over a range of fuel equivalence ratios. Three categories of test were

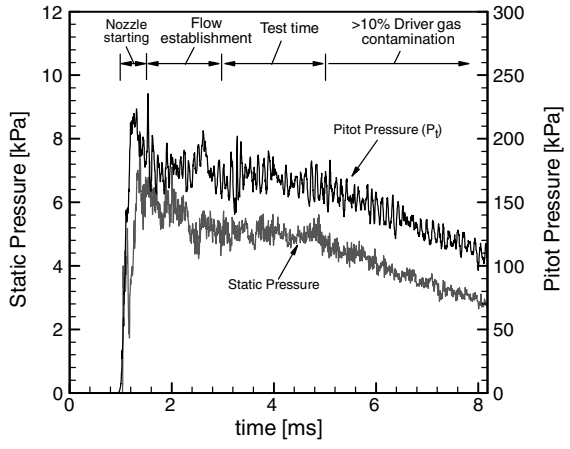

Fig. 7 Time histories of pitot and static pressure in a typical shock-tunnel experiment.

carried out: 1) with air as the test gas and no fuel injection (fuel-off), 2) with air as the test gas and hydrogen fuel injection (fuel-into-air), and 3) with nitrogen as the test gas and hydrogen fuel injection (suppressed combustion). The differences between tests 2 and 3 were used to determine the effects of combustion, and the differences between tests 1 and 3 were used to determine the effects of fuel mass addition. Hydrogen fuel was injected at equivalence ratios up to 1.0.

A. Fuel-Off Results

The measured pressure distributions on the body-side and cowl-side test surfaces for an unfueled experiment, along with numerical predictions, are shown in Fig. 8. Each pressure measurement represents a mean value of the pressure during the test time. The static-pressure measurements were normalized by the measured nozzle supply pressure for each test run (to account for run-to-run variations) and then multiplied by the nominal condition pressure ratio $\bar{p}_s/\bar{p}_1$ so that numerical values are relative to the nominal static pressure entering the engine. The label p/p_1 is used throughout the paper for these normalized pressures. To aid the physical interpretation of the static-pressure data, a correctly scaled representation of the flowpath is also shown. The error bars in Fig. 8 indicate the variation in pressure over the test time. These error bars are typical for the test program and, for clarity, are not included in later plots.

The body-side pressure distribution in Fig. 8 shows a steady rise along the external section of the inlet until the cowl shock reflection labeled RB1, 580 mm from the forebody leading edge. Pressures in the isolator section between RB1 and the 6° bend were relatively constant and indicated a pressure ratio of 18 to 20 for the inlet. This was slightly lower than predicted by the numerical simulation; however, the measurements in this region showed a degree of variation during the test time as indicated by the error bars. The pressure drop at the 6° bend and subsequent shock interaction labeled RB2 showed good agreement with the numerical simulation, indicating that the shock reflection at RB2 produced a pressure ratio of approximately 3.5. Directly behind the RB2 interaction, the combustion-chamber divergence caused a reduction in pressures until the shock interaction RB3, which occurred slightly inside the nozzle. The measured body-side nozzle pressures are closely matched by the numerical simulation.

No pressure data were obtained on the cowl side of the inlet, due to the difficulty in locating pressure transducers. The cowl-side measurements started in the combustion chamber 779 mm downstream of the model leading edge (45 mm downstream of the 6° bend). The initial rise in pressure due to interaction RC1 was not able to be observed; however, the peak measured pressure of $p/p_1 \sim 40$ matched the numerical simulation. The fall in pressure following RC1 occurred slightly upstream compared with the numerical simulation, and this mismatch in shock positions continued further downstream to the shock interaction RC2. In the nozzle, the measured cowl-side pressures were lower than those on the body side and matched the numerical simulation. The overall good match between the measured and numerical pressure distributions gave confidence that the model was properly manufactured, the model was correctly aligned in the tunnel test section, and the inflow conditions were relatively uniform and properly calculated. It is also worth noting that the numerical simulation predicted a core combustion-chamber entrance temperature of about 790 K, too low for self-ignition of a hydrogen and air mixture. Based on the numerical simulations, the inlet had a mass capture ratio of $m_c = 98\%$.

B. Inlet Fuel-Injection Results

The introduction of fuel into the inlet led to some significant changes in the pressure distributions throughout the flowpath. Some were due simply to the gas-dynamic effects associated with injection into a supersonic crossflow, whereas others were due to combustion. Figure 9 shows both the body- and cowl-side pressure distributions for fuel-off suppressed combustion at a simulated equivalence ratio of $\phi = 0.78$ and fuel-into-air at $\phi = 0.80$.

The first feature of note is that the cases with fuel injection (suppressed combustion and fuel-into-air) show a higher body-side pressure in the inlet from $x = 308$ mm (33 mm downstream of injection) onward. It is clear that the barrel shock and other waves caused by the jet-into-crossflow interaction, plus the presence of the hydrogen plume, have changed the inlet pressure distribution. The other phenomenon that could affect the inlet flow (i.e., combustion of fuel in the inlet) was not present, as both the suppressed and fuel-into-air pressure distributions are the same in the inlet.

Moving further downstream, examination of Fig. 9 indicates that ignition occurred at or near interaction RB2. This may be concluded from the divergence between the suppressed and fuel-into-air data that began on the body side at or near RB2. This divergence

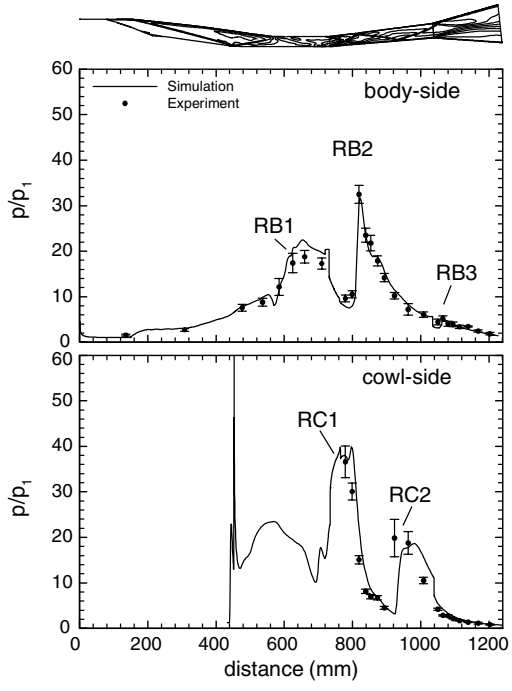

Fig. 8 Axial wall pressure distribution for a typical fuel-off case.

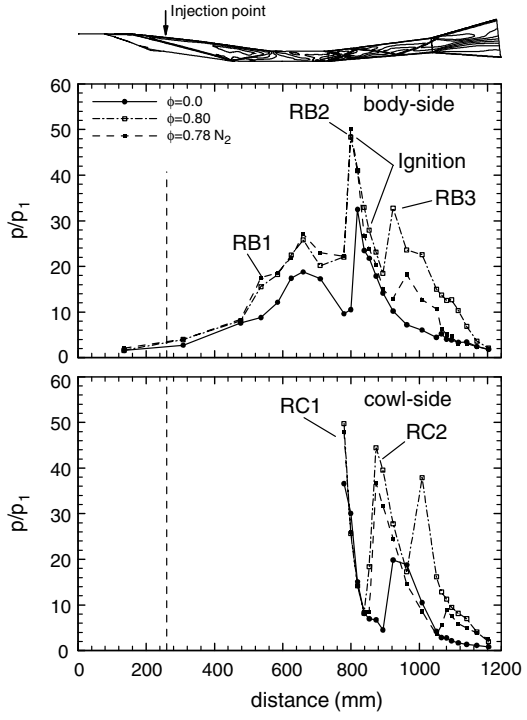

Fig. 9 Comparison of fuel-off, suppressed combustion, and fuel-into-air data.

continued downstream of RB2, with the fuel-into-air body-side pressure levels significantly higher than both the suppressed and fuel-off data throughout the combustion chamber and nozzle. Examination of the cowl-side pressure distribution indicates similar characteristics. These results, which were typical of inlet injection up to $\phi = 0.92$, show the following:

1) No combustion occurred on the inlet.

2) Ignition occurred on the body side of the combustion chamber at RB2.

3) Inlet injection led to substantial pressure rise in the combustion chamber and nozzle of the flowpath.

Figure 10 shows the body- and cowl-side pressure distributions for inlet injection at $\phi = 0.26$, 0.66, and 0.92, along with fuel-off data. It is clear that an increase in ϕ led to an increased pressure rise in the combustion chamber and nozzle, but that the pressure distribution in the inlet remained essentially unchanged. Up to an equivalence ratio of $\phi = 0.92$, it would appear that inlet injection leads to robust ignition and combustion in the flowpath, without disruption to the operation of the inlet.

At high equivalence ratios, however, inlet fuel injection led to unstart of the scramjet flow. Examination of the time histories of unstarted cases indicated that this was initiated in the combustion chamber and fed forward through the isolator to disrupt the inlet flowfield and drastically reduce the engine mass capture. This behavior is believed to be caused by separation of the combustion-chamber flow due to excessive backpressure from the combustion process. The large-scale separation of the boundary layer provided a mechanism for the combustion zone to move forward through the isolator. However, this required fueling at equivalence ratios of $\phi > 0.92$.

There was no evidence of combustion in the inlet for cases with an unseparated boundary layer. A simple injection analysis based on the correlation of Portz and Segal [34] indicated that penetration was four–five times the boundary-layer thickness. Inevitably, some fuel is entrained into the boundary layer, and it is probable that ignition or at least radical production occurred in the heated regions around the fuel injectors. However, the temperature in the bulk of the inlet was too low to sustain combustion, an effect which was demonstrated by Kovachevich et al. [35]. Schwartzentruber and Sislian [36] suggest that ignition in the inlet boundary layer is due to a high-temperature region between the injectors. The interaction of axial vortices from adjacent plumes results in the fuel/air mixture being entrained in this high-temperature region. The wide injector spacing of 25 mm used in this study is in excess of that suggested to avoid this effect.

It is of interest to estimate the level of combustion efficiency corresponding to the inlet-injection pressure distributions shown in Fig. 10. These estimates were obtained here through quasi-1-D cycle-analysis calculations using the code described in Sec. V. In a typical calculation, 1-D stream-thrust conserved properties were determined at the throat of the inlet from the fuel-off numerical simulation, and the addition of fuel in the inlet was modeled by adding the mass, momentum, and total enthalpy of the fuel just downstream of the throat. To model the fact that ignition did not occur in the experimental data until interaction RB2 in the combustion chamber, fuel and air were not allowed to react until this point was reached. Between RB2 and the end of the combustion chamber, fuel and air were allowed to react at a level dictated by a linear combustion-efficiency curve that reached a maximum at the end of the combustion chamber, $\eta_{c,\max}$. No combusting was allowed in the nozzle, which was simply modeled as a 1-D expansion of a mixture of fuel, air, and combustion products. Drag and heat loss to the engine were modeled by assuming an overall skin-friction coefficient $C_f = 0.0025$, use of Reynolds analogy to determine C_h, and a wall temperature $T_w = 300$ K. A value of $\eta_{c,\max}$ was chosen that best matched the average of the experimental body- and cowl-side pressure distributions.

Figure 11 shows comparisons of the experimental data and the 1-D predictions for suppressed ($\phi = 0.78$) and fuel-into-air ($\phi = 0.80$) data. For the suppressed case (where no combustion was allowed), the cycle-analysis calculation did not model the sharp pressure fluctuations due to shock interactions in the real flow, but supplied a reasonable prediction of the average pressure distributions. For the fuel-into-air case, $\eta_{c,\max} = 0.55$ was found to best match the experimentally determined thrust. As shown in Fig. 11, this produced a pressure rise after the ignition point at RB2 that is a reasonable match to the data. It also produced a close match to the pressure rise measured in the nozzle. Based on this comparison, approximately 55% of the injected fuel was combusted, which, in this instance, corresponded to approximately 44% of the captured air being consumed. Based on similar calculations for a range of equivalence

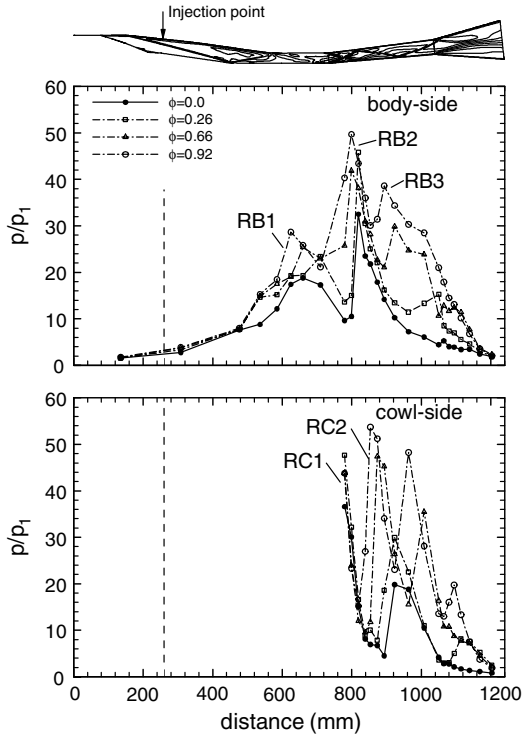

Fig. 10 Comparison of fuel-into-air data at different equivalence ratios.

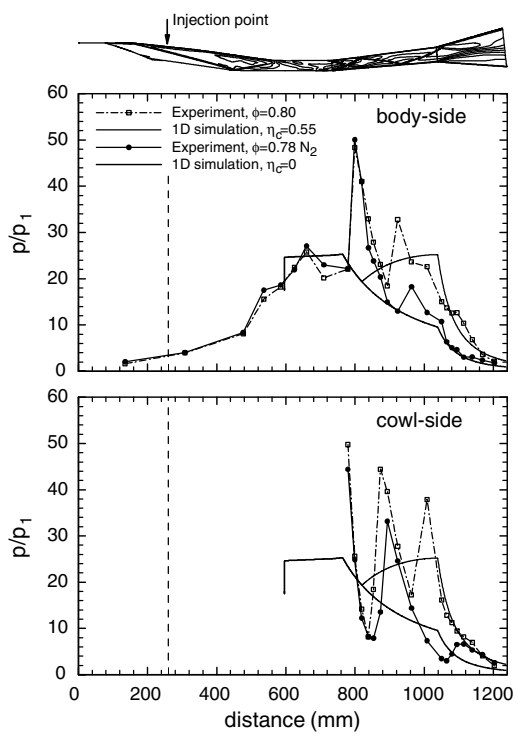

Fig. 11 Comparison of inlet-injection data with cycle-analysis calculations.

ratios, $\eta_{c,\max}$ did not vary greatly with equivalence ratio, and a level of $\eta_{c,\max} \sim 60\%$ was typical of all inlet-injection cases up to $\phi = 0.92$.

Although a combustion efficiency of 60% is a reasonable result for an exploratory study, a value of 80% and above is desirable. Given that the combustion chamber was designed to be long enough to complete the combustion reaction, it is expected that the maximum combustion efficiency is limited in this instance by the mixing of the fuel plumes from the port holes in the inlet. Examination of the expected penetration and spread of the fuel plumes suggests that the fuel does not come into contact with all the captured air. In particular, it does not reach the air on the cowl side of the engine. It is suggested, therefore, that the body-side inlet injection used in the current study should be supplemented by either 1) fuel injection on the cowl side of the inlet or 2) fuel injection around the elliptical perimeter of the combustion-chamber entrance, in order to obtain a higher combustion efficiency.

C. Estimates of Flowpath Thrust Potential

The overall performance of the flowpath was characterized using a coefficient of thrust potential, C_T. This coefficient was calculated using the best available estimate of the thrust force generated by the internal surfaces of the flowpath and is referred to as a coefficient of thrust potential, because the flowpath only included a generic low-expansion-ratio nozzle. Installation of a realistic nozzle would be required to determine the actual propulsive capability of the flowpath; however, thrust potential is a valid parameter to use for determining the usefulness of particular fuel-injection schemes. C_T was calculated as

$$C_T = \frac{T_{\text{potential}}}{q_0 A_0} \tag{1}$$

where the thrust potential $T_{\text{potential}}$ is the summation of internal flowpath forces in the flight direction, q_0 is the flight dynamic pressure, and A_0 is the area of the freestream capture stream tube.

The thrust potential has contributions from internal forces on the three main components of the scramjet, i.e., the REST inlet, the combustion chamber, and the nozzle. The vector components of these forces in the flight direction (6 deg different from the facility nozzle axis in the experiments) contribute to $T_{\text{potential}}$, whereas the vector components normal to the flight direction contribute to lift. Both experimental pressure measurements and the fuel-off numerical simulation were used to obtain an estimate of thrust potential in this instance. The fuel-off numerical simulation was used to obtain an estimate of viscous forces with and without fuel injection, as no skin-friction measurements were undertaken in the experiment. The assumption here is that mixing and combustion does not alter the skin friction in the in the scramjet. This approach was taken because it simplifies the analysis and was considered reasonable in light of the experiments of Tanno et al. [37]. These experiments indicate that skin friction in a hypersonic boundary layer is insensitive to mixing and combustion, a similar result was shown by Goyne et al. [38].

It was desired, however, to use the experimental pressure measurements (suitably integrated over the internal flowpath area) to calculate an estimate of inviscid forces. The only difficulty associated with this was the lack of pressure taps on the cowl side of the inlet. The fuel-off numerical simulation was used to overcome this limitation in a process that involved the creation of a series of artificial pressure taps on the cowl side of the inlet at similar axial positions to the body-side taps. When the flowpath was unfueled, the pressure level at the artificial taps was set equal to the fuel-off numerical simulation. With the cowl side of the inlet divided into pre- and postshock integration areas, this methodology resulted in a drag estimate for the unfueled flowpath within 10% of the fuel-off numerical simulation.

Fuel addition in the inlet caused an increase in the measured body-side pressure distribution in the inlet and increased both the body- and cowl-side distributions measured in the combustion chamber and nozzle. The effect of inlet fuel addition on the artificial cowl-side inlet pressure distribution was modeled by increasing the pressure at the artificial pressure taps by the same ratio that the adjacent body-side tap was increased by fuel addition. It is of interest to obtain an estimate of the increase in the inlet wave drag due to fuel injection, ΔD_i, using this methodology. Calculations indicated that ΔD_i was approximately 20% of the fuel-off inlet wave drag at the lowest equivalence ratio tested ($\phi = 0.26$) and increased slowly to a maximum of 40% as the fuel level was increased to the point at which unstart occurred. Although this increase in wave drag due to injection appears significant, as a proportion of the total drag on the inlet, it is modest: between 14 and 22%. This moderate increase in inlet drag with equivalence ratio is consistent with the fact that the increase was due to changes in the wave structure of the inlet from the presence of the fuel plumes and not due to combustion. Figure 12 shows a plot of inlet drag coefficient C_{Di} variation with ϕ, highlighting the contribution of ΔD_i. Two cases of suppressed combustion are included in Fig. 12, showing no significant difference compared with the fuel-into-air cases at similar ϕ.

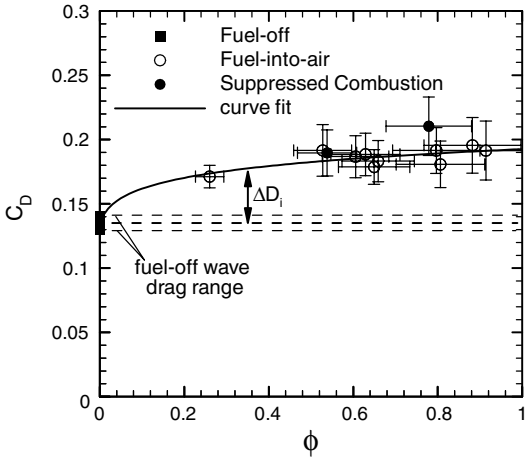

Fig. 12 Inlet wave drag variation with equivalence ratio.

Figure 13 shows plots of C_T versus equivalence ratio, along with thrust predictions from quasi-one-dimensional combustion modeling. The combustion modeling was carried out over a range of $\eta_{c,\max}$ from 0.1 to 1.0. Comparison with the estimated thrust coefficients from the experiments provided an indication of the fuel-based combustion efficiency achieved in the experiments. The C_T values include the viscous drag from the fuel-off numerical simulation and wave drag, including the effect ΔD_i based on the curve fit shown in Fig. 12. With no fuel injection the flowpath had a net drag corresponding to $C_T = -0.15$. Inlet injection increases C_T in an approximately linear fashion, producing a positive C_T at $\phi \sim 0.5$ and a maximum $C_T = 0.18$ at $\phi = 0.92$. For the region of positive C_T, the combustion efficiencies were largely independent of equivalence ratio at approximately $\eta_{c,\max} = 0.6$, with higher values reaching

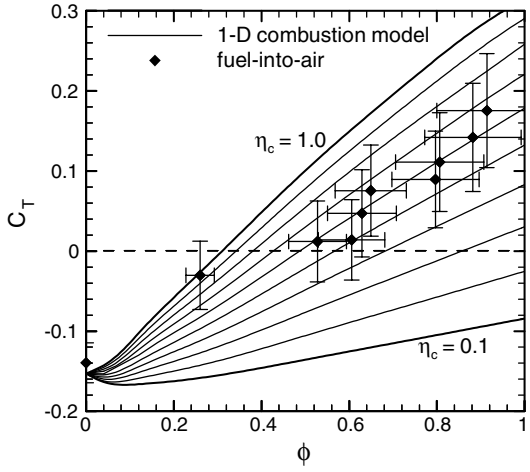

Fig. 13 Variation of thrust potential coefficient with equivalence ratio.

almost 0.7. Since the fuel was injected only on the body side of the inlet, it is believed that improved fuel distribution by complementary injection on the cowl side of the engine would produce an increase in combustion efficiency. Based on these results, it would appear that inlet injection is an effective injection scheme, despite the increased drag produced in the inlet. The main limitation of inlet injection in this flowpath appears to be the occurrence of engine unstart at equivalence ratios less than one.

VII. Conclusions

An experimental investigation of inlet injection in a 3-D scramjet has been conducted at conditions simulating Mach 8.1 flight and 32 km altitude. The 3-D scramjet had a self-starting REST inlet with a geometric contraction ratio of 5.80 and a divergent elliptical combustion chamber with an area ratio of 2.0. The flowpath was completed with a generic nozzle of elliptical cross section with an area ratio of 5.0. Hydrogen fuel was injected in the forward portion of the inlet through multiple portholes that provided a significant fuel/air mixing length upstream of the combustion chamber. This enabled the combustion-chamber length to be sized solely for the completion of the combustion reaction. A fluid-dynamic ignition scheme that made use of shock and expansion waves in the combustion chamber to generate high-temperature regions was used to ignite the fuel without the use of physical obstructions to the flow. The goal of this exploratory study was to determine the usefulness of inlet injection in a flight-style scramjet.

Based on the results of these experiments, it is concluded that inlet injection, in combination with a fluid-dynamic igniter, produced robust combustion of hydrogen fuel at moderate combustion efficiency up to a fuel equivalence ratio slightly less than one. The particular conclusions that may be noted are as follows:

1) Fuel injection in the forward portion of the inlet did not disrupt its operation; however, it did increase the overall drag of the inlet.

2) Although fuel injection changed the pressure distribution in the 3-D inlet, no evidence of combustion was observed in the inlet.

3) The fluid-dynamic scheme used for ignition of the hydrogen fuel was successful for all equivalence ratios tested.

4) Calculated combustion-efficiency levels of approximately 60% were found to be independent of fuel equivalence ratio. It is expected that improved combustion efficiency could be achieved by addition of a secondary fuel-injection station either on the cowl side of the inlet or at the entrance to the combustion chamber.

5) Fueling at equivalence ratios greater than 0.92 led to unstart of the flowpath. Based on time histories of the data, these unstarts were initiated in the combustion chamber and were caused by large-scale combustion-generated flow separation.

6) Inlet injection produced a positive net thrust potential in the flowpath at equivalence ratios greater than 0.5.

The promising results of this study indicate that inlet injection can be a very useful methodology for scramjets operating at higher hypersonic conditions, in which fuel/air mixing length significantly limits overall thrust generation.

Acknowledgment

This research was supported by the Australian Research Council under grant DP0452374.

References

[1] Curran, E. T., "Scramjet Engines: The First Forty Years," *Journal of Propulsion and Power*, Vol. 9, No. 14, 1993, pp. 499–514. doi: 10.2514/2.5875

[2] Townend, L. H., "Domain of the Scramjet," *Journal of Propulsion and Power*, Vol. 17, No. 6, 2001, pp. 1205–1213. doi:10.2514/2.5865

[3] Seiner, J. M., Dash, S. M., and Kenzakovich, D. C., "Historical Survey on Enhanced Mixing in Scramjet Engines," *Journal of Propulsion and Power*, Vol. 17, No. 6, 2001, pp. 1273–1286. doi:10.2514/2.5876

[4] Rogers, C. R., "A Study of Mixing of Hydrogen Injected Normal to a Supersonic Airstream," NASA TN D-6114, March 1971.

[5] Torrence, M. G., "Concentration Measurements of an Injected Gas in a Supersonic Stream," NASA TN D-3860, April 1967.

[6] Torrence, M. G., "Effect of Injectant Molecular Weight on Mixing of a Normal Jet in a Mach 4 Airstream," NASA TN D-6061, Jan 1971.

[7] McClinton, C. R., "The Effect of Injection Angle on the Interaction Between Sonic Secondary Jets and a Supersonic Freestream," NASA TN D-6669, 1972.

[8] Billig, F. S., Orth, R. C., and Lasky, M., "A Unified Analysis of Gaseous Jet Penetration," *AIAA Journal*, Vol. 9, June 1971, pp. 1048–1058. doi:10.2514/3.49916

[9] Gruber, M. R., Baurle, R. A., Mathur, T., and Hsu, K. Y., "Fundamental Studies of Cavity-Based Flameholder Concepts for Supersonic Combustors," *Journal of Propulsion and Power*, Vol. 17, No. 1, 2001, pp. 146–153. doi:10.2514/2.5720

[10] Baurle, R. A., and Eklund, D. R., "Analysis of Dual-Mode Hydrocarbon Scramjet Operation at Mach 4-6.5," *Journal of Propulsion and Power*, Vol. 18, No. 5, 2002, pp. 990–1002. doi:10.2514/2.6047

[11] Henry, J. R., and Anderson, G. Y., "Design Considerations for the Airframe Integrated Scramjet," NASA TM X-2895, 1973.

[12] Donahue, J. M., McDaniel, J. C., and Haj-Hariri, H., "Experimental and Numerical Study Of Swept Injection into a Supersonic Flowfield," *AIAA Journal*, Vol. 32, No. 9, 1994, pp. 1860–1867. doi:10.2514/3.12184

[13] Riggins, D. W., McClinton, C. R., Rogers, R. C., and Bittner, R. D., "Investigation of Scramjet Strategies for High Mach Number Flows," *Journal of Propulsion and Power*, Vol. 11, No. 3, 1995, pp. 409–418. doi:10.2514/3.23859

[14] Guoskov, O. V., Kopchenov, V. I., Lomkov, K. E., Vinogradov, V. A., and Waltrup, P. J., "Numerical Research of Gaseous Fuel Preinjection in Hypersonic Three-Dimensional Inlet," *Journal of Propulsion and Power*, Vol. 17, No. 6, 2001, pp. 1162–1169. doi:10.2514/2.5890

[15] Gardner, A. D., Paull, A., and McIntyre, T. J., "Upstream Porthole Injection in a 2D Scramjet Model," *Shock Waves*, Vol. 11, No. 5, 2002, pp. 369–375. doi:10.1007/s001930200120

[16] Odam, J., "Scramjet Experiments Using Radical Farming," Ph.D. Dissertation, Mechanical Engineering Dept., Univ. of Queensland, Brisbane, Australia, 2004.

[17] McGuire, J. R., "Ignition Enhancement for Scramjet Combustion," Ph.D. Dissertation, Univ. of New South Wales, Sydney, Australia, 2007.

[18] Odam, J., and Paull, A., "Comparison of Experimental Thrust Measurements with Theoretical Values for a Scramjet Engine," 12th AIAA International Space Planes and Hypersonic Systems and Technologies, AIAA Paper 2003-6961, Dec. 2003.

[19] Smart, M. K., "Design of Three-Dimensional Hypersonic Inlets with Rectangular-to-Elliptical Shape Transition," *Journal of Propulsion and Power*, Vol. 15, No. 3, 1999, pp. 408–416. doi:10.2514/2.5459

[20] Smart, M. K., and Ruf, E. G., "Free-Jet Testing of a REST Scramjet at Off-Design Conditions," AIAA Paper 2006-2955, June 2006.

[21] Smart, M. K., Hass, N. E., and Paull, A., "Flight Data Analysis of the HyShot 2 Scramjet Flight Experiment," *AIAA Journal*, Vol. 44, No. 10, 2006, pp. 2366–2375. doi:10.2514/1.20661

[22] Smart, M. K., "Experimental Testing of a Hypersonic Inlet with Rectangular-to-Elliptical Shape Transition," *Journal of Propulsion and Power*, Vol. 17, No. 2, 2001, pp. 276–283. doi:10.2514/2.5774

[23] Pergament, H. S., "Theoretical Analysis of Nonequilibrium Hydrogen-Air Reactions in Flow Systems," *AIAA-ASME Hypersonic Ramjet Conference*, Paper 63113, 1963.

[24] Stalker, R. J., Paull, A., Mee, D. J., Morgan, R. G., and Jacobs, P. A., "Scramjets and Shock Tunnels—The Queensland Experience," *Progress in Aerospace Sciences*, Vol. 41, No. 6, 2005, pp. 471–513. doi:10.1016/j.paerosci.2005.08.002

[25] Smith, A. L., "Multiple Component Force Balance Measurement in Short Duration Test Flows," Ph.D. Dissertation, Dept. of Mechanical Engineering, Univ. of Queensland, Brisbane, Australia, 1999.

[26] McIntosh, M. K., "Computer Program for the Numerical Calculations of Frozen and Equilibrium Conditions in Shock Tunnels," Australian National Univ., Canberra, ACT, Australia, 1968.

[27] Paull, A., "A Simple Shock-Tunnel Driver Gas Detector," *Shock Waves*, Vol. 6, No. 5, 1996, pp. 309–312. doi:10.1007/s001930050049

[28] Skinner, K. A., "Mass Spectrometry in Shock Tunnel Experiments of Hypersonic Combustion," Ph.D. Dissertation, Dept. of Mechanical

Engineering, Univ. of Queensland, Brisbane, Australia, 1994.
[29] White, J. A., and Baurle, R. A., "Viscous Upwind Algorithm for Complex Flow Analysis, User Manual," Ver. 4.5.3, NASA Langley Research Center, Hampton, VA, 2007.
[30] Smart, M. K., and White, J. A., "Computational Investigation of the Performance and Back-Pressure Limits of a Hypersonic Inlet," 40th Aerospace Sciences Meeting and Exhibit, AIAA Paper 2002-0508, Jan. 2002.
[31] Baurle, R. A., and Gaffney, R. L., "Extraction of One-Dimensional Flow Properties from Multidimensional Data Sets," *Journal of Propulsion and Power*, Vol. 24, No. 4, 2008, pp. 704–714. doi:10.2514/1.32074
[32] Smart, M. K., "Scramjets," *The Aeronautical Journal*, Vol. 111, No. 1124, 2007, pp. 605–619.
[33] Shapiro, A. H., *The Dynamics and Thermodynamics of Compressible Fluid Flow*, Wiley, New York, 1953.
[34] Portz, R., and Segal, C., "Penetration of Gaseous Jets in Supersonic Flows," *AIAA Journal*, Vol. 44, No. 10, 2006, pp. 2426–4268. doi:10.2514/1.23541
[35] Kovachevich, A., Paull, A., and McIntyre, T., "Investigation of an Intake Injected Hot-Wall Scramjet," 42nd AIAA Aerospace Sciences Meeting and Exhibit, AIAA Paper 2004-1037, Jan. 2004.
[36] Schwartzentruber, T. E., and Sislian, J. P., "Suppression of Premature Ignition in the Premixed Inlet Flow of a Scramjet," *Journal of Propulsion and Power*, Vol. 21, No. 1, 2005, pp. 87–94. doi:10.2514/1.7003
[37] Tanno, H., Paul, A., and Stalker, R. J., "Skin-Friction Measurements in a Supersonic Combustor with Crossflow Fuel Injection," *Journal of Propulsion and Power*, Vol. 17, No. 6, 2001, pp. 1333–1338. doi:10.2514/2.5883
[38] Goyne, C. P., Stalker, R. J., and Paull, A., "Shock-Tunnel Skin-Friction Measurement in a Supersonic Combustor," *Journal of Propulsion and Power*, Vol. 15, No. 5, 1999, pp. 699–705. doi:10.2514/2.5481

T. Jackson
Associate Editor